

# First principles investigation of defect emission from hBN

Sherif Abdulkader Tawfik\*,<sup>1</sup> Sajid Ali\*,<sup>1,2</sup> Marco Fronzi,<sup>1,3</sup> Mehran Kianinia,<sup>1</sup> Toan Trong Tran,<sup>1</sup> Catherine Stampfl,<sup>4</sup> Igor Aharonovich,<sup>1</sup> Milos Toth,<sup>1</sup> and Michael J. Ford<sup>1,\*</sup>

<sup>1</sup>*School of Mathematical and Physical Sciences, University of Technology Sydney, Ultimo, New South Wales 2007, Australia*

<sup>2</sup>*Department of Physics, GC University Faisalabad, Allama Iqbal Road, 38000 Faisalabad, Pakistan*

<sup>3</sup>*International Research Centre for Renewable Energy,*

*State Key Laboratory of Multiphase Flow in Power Engineering,*

*Xi'an Jiaotong University, Xi'an 710049, Shaanxi, China*

<sup>4</sup>*School of Physics, The University of Sydney, New South Wales, 2006, Australia*

Hexagonal boron nitride (hBN) has recently emerged as a fascinating platform for room-temperature quantum photonics due to the discovery of robust visible light single-photon emitters. In order to utilize these emitters, it is necessary to have a clear understanding of their atomic structure and the associated excitation processes that give rise to this single photon emission. Here we perform density-functional theory (DFT) and constrained DFT calculations for a range of hBN point defects in order to identify potential emission candidates. By applying a number of criteria on the electronic structure of the ground state and the atomic structure of the excited states of the considered defects, and then calculating the Huang-Rhys (HR) factor, we find that the  $C_B V_N$  defect, in which a carbon atom substitutes a boron atom and the opposite nitrogen atom is removed, is a potential emission source with a HR factor of 1.66, in good agreement with the experimental HR factor. We calculate the photoluminescence (PL) line shape for this defect and find that it reproduces a number of key features in the the experimental PL lineshape.

## I. INTRODUCTION

Fluorescent defects in solids have attracted considerable attention as promising qubits for quantum information science.<sup>1–4</sup> While the nitrogen vacancy ( $N_V^-$ ) center in diamond has been widely investigated<sup>5</sup>, other emerging defects are far less understood. One particular example is the recently discovered single photon emitters in mono and multi-layer hexagonal boron nitride (hBN).<sup>6–20</sup> While the emission was independently observed by several groups, the crystallographic structure of the defects and their origin are still under debate.

Prior to this discovery, hBN has mainly been examined for ultraviolet emission. Such emission was attributed to grain boundaries<sup>20,21</sup> and point defects,<sup>20</sup> in particular N vacancies and carbon defects,<sup>22,23</sup> and oxygen defects.<sup>24</sup> As for the newly discovered visible single-photon emission (SPE) from hBN, based on *ab initio* calculations, the nitrogen anti-site defect was proposed as a potential candidate.<sup>7,8</sup> Given that SPE from hBN would emerge from isolated point defects, and that it is possible to engineer defects using a variety of experimental techniques, such as scanning tunnelling microscopy,<sup>25</sup> the identification of the nature of these defects at an atomic level will be of great benefit for the control and reproducibility of these emitters as well as understanding and predicting their physical and chemical properties.

The formation and stability of a number of hBN defects have been examined in the literature using conventional density-functional theory (DFT) approaches, for example native defects,<sup>26–29</sup> boron-terminated tetravacancies,<sup>30</sup> oxygen-stabilized triangular voids,<sup>31</sup> substitutional C defects,<sup>28,29</sup> and StoneWales defects with an without a C impurity.<sup>32</sup> The formation of certain substitutional C defects are predicted to be more stable than native de-

fects by analysing the formation energies,<sup>28,29</sup> but the presence of C dopants favors the formation of C-doped StoneWales defects.<sup>32</sup> In addition, the presence of oxygen greatly stabilizes multi-atom vacancies.<sup>31</sup> Here we focus on 36 defects including native defects, doping with F, P, S, Si O, and C, and the Stone-Wales (SW) defect with and without C doping. Among those defects are 8 O oxygen-based defects, owing to the role of oxygen in stabilizing vacancies, and 8 Si-based defects, in order to account for the possibility that Si atoms from the substrate might bind to hBN vacancies.

In addition to using ground-state DFT to explore the electronic structure of these defects we have also calculated the PL line shapes using the approach first introduced by Alkauskas *et al.*<sup>49</sup> and applied for GaN and ZnO, and later to  $NV^-$  diamond.<sup>33</sup> This approach is an extension of the quantum mechanical model proposed by Huang and Rhys in their seminal paper,<sup>34</sup>. There is now an extensive literature applying their method to a wide range of luminescent defects (see Ref. 35–37). A key quantity in the Huang-Rhys method is the Huang-Rhys (HR) factor, which quantifies coupling between the electronic and vibronic states and gives a measure of the strength of the phonon side bands (PSB) relative to the zero-phonon line (ZPL). A technologically useful single photon source requires a small HR factor. Applying the HR theory requires the prediction of the excited state (ES) geometry and the phonon modes of the system including those associated with the presence of a defect. Excited state geometries can be calculated using constrained DFT (or  $\Delta SCF$ <sup>38</sup>) where one electron is held in an excited state while the atomic positions are relaxed.

In this paper, we apply the combined DFT-CDFT method to identify the defects that are most likely the emission sources of hBN. We utilize the formalism of op-

tically active centers in solids in order to evaluate the Huang-Rhys (HR) factor for the most likely defect structures, and subsequently obtain the PL lineshape for those structures. We find that a C-antisite defect ( $V_N C_B$ ), is a promising candidate, given that its HR factor is identical to the experimentally obtained one, and its theoretical PL spectrum is in reasonable agreement with the experimental PL spectrum of emitters.

## II. THEORETICAL METHOD

We performed density functional-theory (DFT) calculations of point defects in hBN in order to assign the observed single-photon emission to specific point defects. The calculations were performed using SIESTA<sup>39</sup> and VASP.<sup>40</sup> Our SIESTA and VASP calculations were performed using the generalized gradient approximation by Perdew, Burke and Ernzerhof (PBE).<sup>41</sup> For the PBE calculations, we used a supercell that is comprised of  $7 \times 7$  unit cells of hBN (98 atoms), and we performed geometry relaxation for obtaining the ground state electronic structure with a  $3 \times 3 \times 1$   $\mathbf{k}$ -grid in both DFT codes. SIESTA uses basis sets comprised of numerical atomic orbitals, and approximates the ionic potential in terms of Troullier-Martins<sup>42</sup> norm-conserving pseudopotentials. The auxiliary basis uses a real-space mesh with a kinetic energy cutoff of 750 Ry, and the basis functions are radially confined using an energy shift of 0.005 Ry. In the structural energy minimization, the internal coordinates are allowed to relax until all of the forces are less than 0.02 eV/Å. A vacuum region of 20 Å is added between the periodic images. In VASP, the valence electrons are separated from the core by use of projector-augmented wave pseudopotentials (PAW).<sup>43</sup> The energy cut-off for the plane wave basis set is 500 eV, and the energy tolerance is  $10^{-6}$  eV. In the structural energy minimization, the internal coordinates are allowed to relax until all of the forces are less than 0.01 eV/Å. A vacuum region of 15 Å is added between the periodic images. The lattice constant of the hBN primitive cell is  $a = 2.515$  Å using both SIESTA and VASP, calculated on a  $8 \times 8 \times 1$   $\mathbf{k}$ -grid. Phonon calculations were performed using the Phonopy code.<sup>44</sup>

We have performed CDFT calculation using both SIESTA and VASP for comparison. CDFT for the defect structures is performed by promoting an electron from the occupied defect state to the next unoccupied defect state of the same spin-polarization, assuming that the transition is spin-preserving. This is a widely applied technique for simulating optical excitation in molecules and crystals, and allows us to calculate the ZPL energy.<sup>38,45–47</sup> In the SIESTA CDFT calculation, we have used a single  $\Gamma$  point: Given that, in the ground state SIESTA calculation, the difference in total energy between using a single  $k$  point and a  $3 \times 3$   $k$ -point grid is  $10^{-3}$  eV, this justifies using a single  $\mathbf{k}$  point in excited state calculation and a  $3 \times 3 \times 1$   $\mathbf{k}$ -grid in the

ground state calculations.

The HR factor is calculated by applying the one-dimensional configuration coordinate formulation, and the PL spectral function  $L(\hbar\omega)$  is obtained following the generating function procedure,<sup>33,48,49</sup> starting from

$$L(\hbar\omega) = C\omega^3 A(\hbar\omega) \quad , \quad (1)$$

where  $A(\hbar\omega)$  is the optical spectral function and is related to the electron-phonon spectral function,  $S(\hbar\omega)$ , and the ZPL,  $C$  is a normalization constant (details in the Supplementary Information). The function  $S(\hbar\omega)$  is defined as follows:

$$S(\hbar\omega) = \sum_k S_k \delta(\hbar\omega - \hbar\omega_k) \quad , \quad (2)$$

$\omega_k$  is the phonon frequency and  $S_k$  is the partial HR factor. The Dirac delta function is approximated here as a gaussian with width  $\sigma$ .  $S_k$  is given by

$$S_k = \frac{\omega_k}{2\hbar} q_k^2 \quad , \quad (3)$$

where  $q_k$  is given by

$$q_k = \sum_{ai} m_a^{1/2} (R_{e,ai} - R_{g,ai}) \Delta r_{k,ai} \quad , \quad (4)$$

where  $a$  enumerates the atoms,  $i = x, y, z$ ,  $m_a$  is the atomic mass of species  $a$ ,  $R_{g/e,ai}$  is the position of atom  $a$  in the ground/excited state, and  $\Delta r_{k,ai}$  is the atomic displacement in normal coordinates. The total HR factor is then given by

$$S = \sum_k S_k \quad . \quad (5)$$

In order to evaluate the Huang-Rhys factor from the experimental data, we utilize the relationship between  $S$  and the intensity of the ZPL,  $I_0$ :

$$S = -\ln(I_0^T / I^T) \quad , \quad (6)$$

where  $I_0^T$  is the area under the ZPL line, while  $I^T$  is the integral of the full PL lineshape.<sup>50</sup> A measure of the extent of atomic structure change due to excitation is represented by the quantity  $\Delta Q$  which is defined by the formula:

$$\Delta Q^2 = \sum_{ai} m_a^{1/2} (R_{e,ai} - R_{g,ai}) \quad . \quad (7)$$

### III. RESULTS AND DISCUSSION

#### A. Defect Electronic Structures

For the 36 point defect structures listed in Tab. 1, we have calculated the imaginary component of the dielectric constant and the band structure in the ground state (GS) in order to identify promising defects with emission properties consistent with the experiments. Defects labeled Si- $n$  are Si-based defects with complex structure, and  $\text{SWC}_N$  is the Stone-Wales defect in which an N atom is substituted for a C atom. The values of  $E_T^{\uparrow\downarrow}$  correspond to characteristic peaks in the imaginary dielectric function (effectively peaks in the optical absorption spectrum) for the spin-up and spin-down channels respectively. To select potential emitters, we have applied 3 criteria, based on experimental observations, in order to narrow down the list of potential defects shown in Tab. 1:

1. The stability of the emitters against annealing<sup>8</sup> and high temperature<sup>12</sup> imply that the positions of the defect levels are within the band gap, and that none of them reside within, or close to, the bulk bands.<sup>47</sup>
2. The observed emitters are polarized,<sup>7</sup> and therefore we only focus on defects in which the defect excitation in the optical spectrum is also polarized.
3.  $E_{ZPL}$  is between 1.3 eV and 2.0 eV, which includes the range of ZPL energies reported in the literature.<sup>7-9,19</sup> It is important to remember the limitations of DFT in this regard where it is well known that band-gaps in semiconductors are underestimated relative to experimental values.

A subset of the considered defects are presented in Tab. 2. In the defects of Tab. 2,  $E_T^{\uparrow\downarrow}$  lies within the band gap, and criteria (1) and (2) are satisfied. Then, applying criterion (3) on the defects in Tab. 2, we found that there are three defect structures that could potentially emit single photons: the N-anti-site defect ( $\text{N}_B\text{V}_N$ ) presented in Fig. 1(a) ( $\Delta Q = 0.66 \text{ amu}^{1/2} \text{ \AA}$ ), the  $2\text{O}_{2B}\text{V}_N$  defect ( $\Delta Q = 0.93 \text{ amu}^{1/2} \text{ \AA}$ ) and the  $\text{C}_B\text{V}_N$  defect ( $\Delta Q = 0.53 \text{ amu}^{1/2} \text{ \AA}$ ). The calculations using VASP gave values for  $E_{ZPL}$  that are very close to the values obtained using SIESTA: 2.01 eV, 1.85 eV and 1.33 eV for the  $\text{N}_B\text{V}_N$ ,  $2\text{O}_{2B}\text{V}_N$  and  $\text{C}_B\text{V}_N$  defects, respectively. The  $\text{S}_B, \text{V}_N\text{C}_B\text{B}_N$ ,  $\text{S}_V\text{B}_N$ , Si-1 and Si-2 defects, although they satisfy the above four criteria, undergo large structural change as quantified by  $\Delta Q$ , as defined in Eq. 7 (for these defects,  $\Delta Q = 4.18, 4.91, 1.45, 9.91$  and  $5.00 \text{ amu}^{1/2} \text{ \AA}$ , respectively). Such large values for  $\Delta Q$  would correspond to large HR values.

The atomic structure of the ground state (GS) and excited state (ES) structures of  $\text{N}_B\text{V}_N$ ,  $2\text{O}_{2B}\text{V}_N$  and  $\text{C}_B\text{V}_N$  defects are presented in Fig. 1(b), (d) and (f), respectively. In all of the structures, there is no out-of-plane displacement upon excitation, which means that

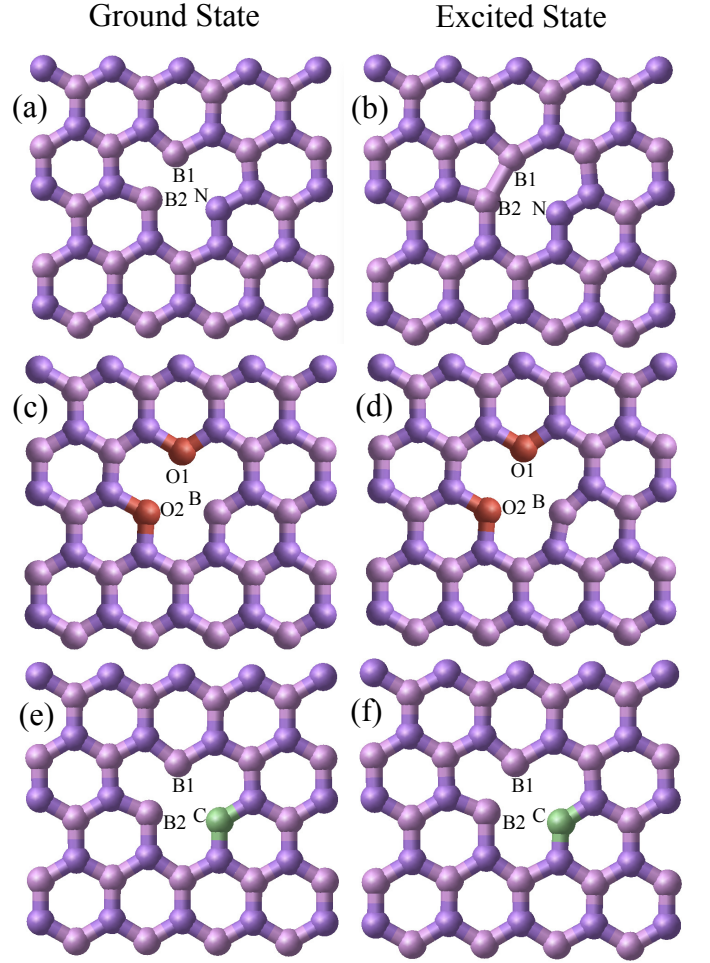


FIG. 1: (Color online) The atomic structure of the ground state (GS) (a) and the excited state (ES) (b) of the  $\text{N}_B\text{V}_N$  defect, GS (c) and ES (d) of the  $2\text{O}_{2B}\text{V}_N$  defect, and GS (e) and ES (f) of the  $\text{C}_B\text{V}_N$  defect. Nitrogen atoms are displayed as violet spheres, B atoms as pink, C as green and O as red. The bond distances in (a) are N-B1/2: 2.59 Å, B1-B2: 1.95 Å, (b) N-B1/2: 2.64 Å, B1-B2: 1.80 Å, (c) B-O1/2: 2.52 Å, O1-O2: 2.53 Å, (d) B-O1/2: 2.68 Å, O1-O2: 2.58 Å, (e) C-B1/2: 2.53 Å, B1-B2: 2.07 Å and (f) C-B1/2: 2.62 Å, B1-B2: 2.00 Å.

the out-of-plane optical phonon modes do not contribute to the partial HR factor (Eq. 3). For  $\text{N}_B\text{V}_N$ , the main difference between the atomic structure of the obtained excited structure (cf. Fig. 1(b)) and that of the ground state structure (cf. Fig. 1(a)) is that the B-B bond distance drops by 0.14 Å; for  $2\text{O}_{2B}\text{V}_N$ , the B-O1/2 stretches by 0.16 Å; for  $\text{C}_B\text{V}_N$ , which undergoes the least atomic displacement, C-B1/2 stretches by 0.09 Å. The atomic structure of the GS for all of the considered structures is available in the Supplementary Information.

TABLE I: The calculated electronic transition energy of the spin-up defect state,  $E_T^\uparrow$ , the spin-down defect state,  $E_T^\downarrow$ , the ZPL energy  $E_{ZPL}$ , the HR factor, and the satisfaction/dissatisfaction of the four criteria of a single-photon source. All energies are in units of eV. The atomic structures of these defects are displayed in the Supplementary Information.

Defect	$E_T^\uparrow$	Bulk bands?	$E_T^\downarrow$	Bulk bands?	Polarized
$C_B$	-		-		
$C_N$	-		-		
$PV_{BN}$	3.41		-		
$SV_{BN}$	2.72	No	2.72	No	Yes
$SiV_{BN}$	2.71	Yes	-		
$F_B$	2	No	2	No	No
$S_B$	2.26	No	-		Yes
$Si_B$	-		-		
$Si_B V_N$	3.28	No	3.28	No	Yes
$Si_N$	-		-		
$S_N$	-		-		
$V_{2N2B}$	-		1.67	Yes	
$V_B$	-		2.31	Yes	
$V_N$	2.08	No	-		No
$2O_{2B}2O_{2N}V_{BN}$	-		-		
$O_B V_N$	-		-		
$2O_{2B}V_N$	2.39	No	-		Yes
$3O_{3B}V_N$	-		-		
$O_N V_B$	-		-		
$2O_{2N}V_B$	-		-		
$3O_{3N}V_B$	-		-		
SW	3.55		3.55		
SWC <sub>N</sub>	2.94	No	-		Yes
SWC <sub>B</sub>	2.02	Yes	-		No
$V_{3N}V_B$	-		-		
$C_N V_B$	1.93		2.67		Yes
$C_B V_N$	1.44	No	-		Yes
$N_B V_N$	2.02	No	-		Yes
$O_2 V_B$	2		0.87, 2.18		Yes
Si-1	2.21		2.21		
Si-2	2.2		-		
Si-3	1.83	No	1.99	No	
Si-4	0.42, 0.96	No	-		
Si-5	3.44, 3.75		-		
$V_N C_B B_N$	1.00	No	1.00	No	Yes
HN	1.75, 2.97	No	-		

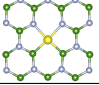
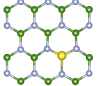
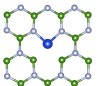
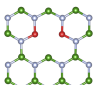
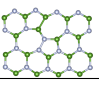
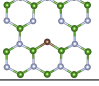
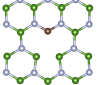
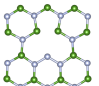
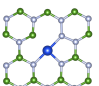
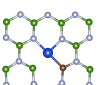
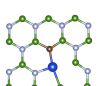
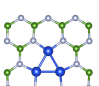
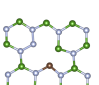
### B. Photoluminescence lineshapes and the Huang-Rhys factors

In our search for potential emitter structures, we have calculated the theoretical HR factors for the four emitters considered in the previous section using SIESTA. The values are: 4.49 for  $N_B V_N$ , 6.74 for  $2O_{2B}V_N$  and 1.66 for  $C_B V_N$ . That is, the emitter whose theoretical HR factor agrees with the experimental HR factor value of the emitter (which we calculated as  $S=1.66$  using Eq. 6) is the  $C_B V_N$ . The HR factors of the other two emitters

are too high compared with the available experimental HR value.

The partial HR factor (Eq. 3), the spectral function of electron-phonon coupling (Eq. 2) and the PL lineshape (Eq. 1) are displayed in Fig. 2 for the two defects,  $C_B V_N$  and  $N_B V_N$ . The theoretical lineshape of  $C_B V_N$  is superimposed on the experimental lineshape with a ZPL at 1.951 eV, which has been measured at 4K (Supplementary Information). The two spectral functions terminate at 200 meV, which is the maximum of the hBN phonon energy. The value of  $\gamma$  has been adjusted in order to fit

TABLE II: The calculated ZPL energy  $E_{ZPL}$  (in eV) and the  $\Delta Q$  for the defects (defined in Eq. 7) in which  $1.6 < E_{ZPL} < 2.2$ . The atomic structures of these defects are displayed in the Supplementary Information. For defects where the  $E_{ZPL}$  do not satisfy criterion (3), we do not show  $\Delta Q$ .

Defect	ZPL (spin-up)	$\Delta Q$	Structure
$SV_{BN}$	1.94	1.45	
$S_B$	1.26	4.18	
$Si_B V_N$	0.94	4.00	
$2O_{2B} V_N$	1.90	0.93	
$SWC_N$	2.70	0.30	
$C_N V_B$	1.11	1.86	
$C_B V_N$	1.39	0.53	
$N_B V_N$	2.12	0.66	
Si-1	1.86	9.91	
Si-2	2.03	5.00	
Si-3	0.62	5.02	
Si-5	3.81	5.03	
$V_N C_B B_N$	2.16	4.91	

the experimental spectrum in Fig. 2(b), and the same value is used in Fig. 2(d). In the experimental spectrum of Fig. 2(a), there are PSB peaks at 1.92 eV, 1.8 eV, 1.76 eV, and 1.75 eV. Using Eq. 6, the HR factor is 1.66. This spectrum resembles that of the 4.1 eV color center of hBN reported in Ref. 20 (measurement made at 10K): a broad low-energy feature right next to the ZPL peak, a peak at the maximum phonon energy of 200 meV and fine structure in between. Although the resemblance between the lineshapes does not imply that the emitting sources have any relationship, it helps to identify the sharp peak at 1.75 eV (200 meV away from the ZPL). This peak has been identified by the authors of Ref. 20 as a zone-center longitudinal optical phonon. Such phonons scale as  $1/k$ , where  $k$  is the phonon wave vector, and therefore the electron-phonon matrix element of these phonons diverge, leading to such intense peak.<sup>20</sup>

We can observe that the spectrum of the  $C_B V_N$  defect has two high-energy features, A and B, corresponding to the two high energy features in the experimental spectrum, but blue-shifted by  $\sim 20$  meV from the corresponding positions in the experimental spectrum. In addition, the theoretical spectrum in Fig. 2(b) exhibits a low energy peak, C, that is  $\sim 10$  meV away from the 1.90 eV peak in the experimental spectrum. On the contrary, the  $N_B V_N$  lineshape considerably deviates from the experimental lineshape: there is a large peak that is  $\sim 470$  meV away from the ZPL. This information strongly suggests that the  $C_B V_N$  defect is one of the SPE sources in hBN.

Next, we analyse the localization-delocalization of phonon modes that contribute to the PL lineshape of the two defects. Although the concept of degree of localization is not well defined for complex structures, it is possible to roughly quantify the degree of localization based on the inverse participation ratio, or IPR<sup>33</sup>. This quantity gives the number of atoms that vibrate in a given normal mode, and ranges from 1 (a single atom vibrating) up to the total number of atoms in the supercell (97 in the case of the three defect structures). For the case of the  $C_B V_N$  defect, we analyze the  $S_k$  function displayed in Fig. 2(a). Three modes represent 55.6% of the total HR factor. The largest contribution is from a mode at 30 meV with  $IPR_k = 70$ , and represents 31.5% of the total HR factor. Then, a slightly localized mode at 46 meV with  $IPR_k = 43$  and represents 14.6%. Then a slightly localized mode at 48 meV with  $IPR_k = 32$  and represents 14.6%. These three phonon modes are illustrated in Fig. 3(a,b,c). Both the 30 meV and the 48 meV phonon modes are defect breathing modes, in which the atoms surrounding the defect oscillate along the dipole direction of the defect. Therefore, they are infrared active modes, because the dipole moment of the defect changes. The 46 meV phonon mode is also a defect breathing mode, but the defect atoms in this mode oscillate radially around the defect site; that is, it is a symmetric breathing mode which is Raman active. A few localized modes with  $IPR_k < 15$  exist at low phonon energy and with negligible contribution to the total HR factor. The



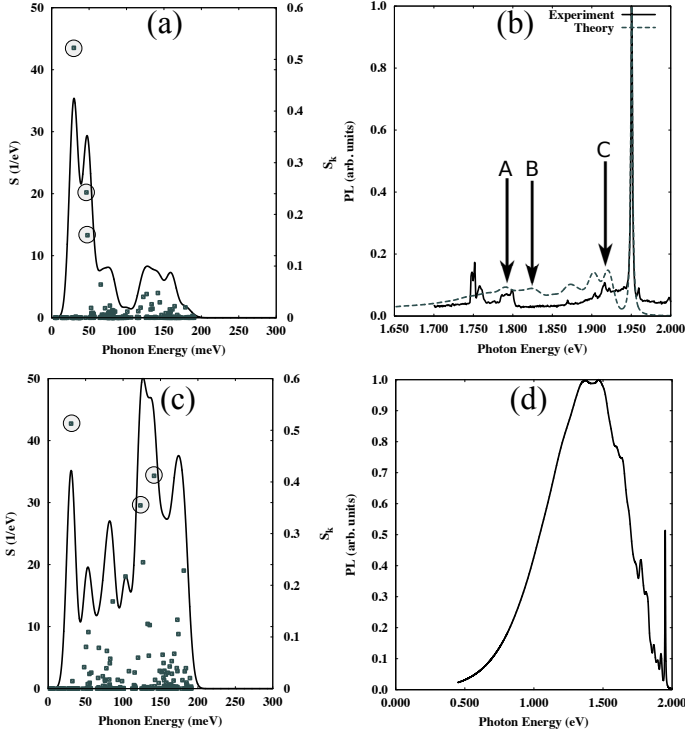


FIG. 2: (Color online) The set of partial HR factors,  $S_k$ , along with the approximate partial HR function,  $S(\hbar\omega)$ , and the photoluminescence lineshape of  $C_B V_N$  defect (a,b) and the  $N_B V_N$  defect (c,d). The experimental spectrum of the emitter is also displayed in (b). The phonon modes labelled with circles in (a) and (c), which have the most significant contribution to the HR value, are displayed in Fig. 3.

localized mode with highest contribution is at 142 meV, with  $IPR_k = 12$  and represents 2.9% of the total HR factor. The high energy peaks that are responsible for the  $S(\omega)$  peak at 150 meV in 2(a) collectively represent 6.8% of the total HR factor and with  $32 < IPR_k < 58$ . This information indicates that phonon modes that contribute to photoluminescence in the  $C_B V_N$  defect are not local modes. This is in agreement with the conclusion in Ref. 20 for the case of UV luminescence.

For the case of the  $N_B V_N$  defect, the peak at 42 meV is a delocalized phonon mode in which the defect site move along the dipole direction, accompanied by the mobility of the majority of the atoms surrounding the defect. This mode has the largest partial HR factor (11.4% of the total HR factor) with an IPR value of  $\sim 70$ . The two modes with next-largest HR contribution have energy values 194 and 169 meV and contributes 17% of the total HR factor, and have IPR values of  $\sim 17$  and  $\sim 20$ , where the largest displacements originate from the atoms surrounding the defect site. These three phonon modes are illustrated in Fig. 3(d,e,f). In the 194 meV mode, the N atom in the defect sites stretches further into the defect site (towards the two B atoms), while in the 169 meV mode the two B atoms in the defect site stretch perpendicular to the dipole direction (where each B atom stretch in a direction

opposite to the other). It is the strong electron-phonon coupling in these two high energy defect phonon modes that is responsible for the large PSB in the lineshape (cf. Fig. 2(d)), and hence the large HR factor.

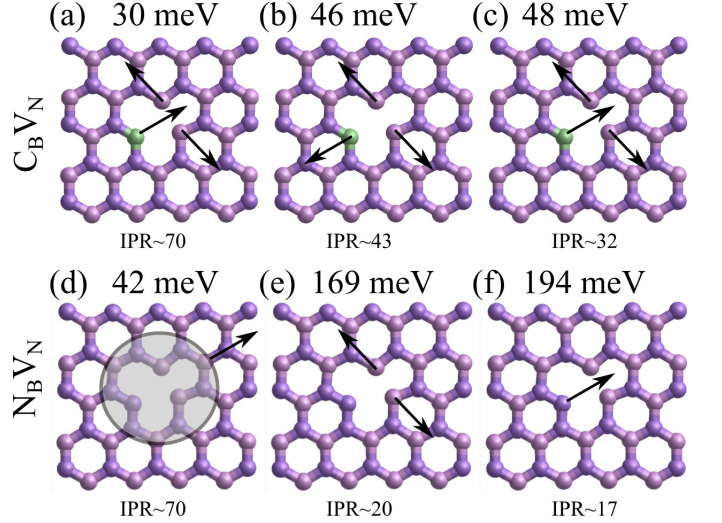


FIG. 3: (Color online) A schematic diagram for the force vectors of the three phonon modes which have the largest contribution to the HR factor for the (a-c)  $C_B V_N$  defect and the (d-f)  $N_B V_N$  defect. In (d), the atoms enclosed by the circle move collectively.

Having applied the quantum theory of F-centers to potential hBN single-photon emitters, it is important to highlight that this theory relies on a number of assumptions and has emerged from the analysis of three-dimensional defect geometries. Therefore, it requires some developments to expand its usefulness for two-dimensional van der Waals crystals, whose physical properties are different from those of three dimensional crystals. If we accept Eq. 4 at face value, then the coupling between electronic excitation and out-of-plane optical phonons will fail to be achieved by a defect in which the optical excitation induces a movement of the atoms in the  $z$ -direction. Algebraically speaking, this problem stems from the very definition of  $S_k$  in terms of the product  $R_{ia,g/e} \Delta r_{ia,k}$ , because it depends on the actual coordinate value of  $R_{ia,g/e}$ . That is, the atoms whose  $z$ -axis coordinate is zero (such as graphene, hBN, etc) will have  $R_{ia,g} \Delta r_{ia,k} = 0$ . If the atoms are displaced along the  $z$ -axis due to optical excitation, then the present theory will incorporate the contribution of optical out-of-plane phonon modes in the electron-phonon coupling by virtue of  $R_{ia,g} \Delta r_{ia,k} \neq 0$ . However, as long as the atoms do not move along the  $z$ -axis, all of the out-of-plane optical modes will not contribute to the electron-phonon coupling, and hence, to the luminescence process. To determine whether this is physically valid, more research on extending the classical F-center theory to 2D materials must be performed. This is currently in progress.

## IV. CONCLUSION

We applied density-functional theory and constrained-density functional theory to hBN in order to predict the luminescence properties of point defects in hBN. The ground state electronic and geometric properties were determined for 36 different defect structures, from which a list of 14 defects were found to satisfy a number of criteria. Only one defect out of this list, the  $C_BV_N$  defect, was found to reproduce the experimental HR factor, and its theoretical PL lineshape is in reasonable agreement with the experimental lineshape. The theoretical analysis of the phonon modes contributing to the PL lineshape of both the  $C_BV_N$  and  $N_BV_N$  defect shows that delocalized modes dominate the PL lineshape in  $C_BV_N$ , which is not the case in the  $N_BV_N$  defect in which the phonon modes with highest contribution are strongly localized. Such localization results in a large phonon-side band contribution in the  $N_BV_N$  defect. Our results provide a fundamental insight in the evolving field of two-dimensional quantum emitters, and will be useful in the engineering

and control of such emitters.

## V. ACKNOWLEDGEMENTS

S. A. T. and S. A. have contributed equally to this work. This research was funded by the Australian Government through the Australian Research Council (ARC DP16010130). The theoretical calculations in this research were undertaken with the assistance of resources from the National Computational Infrastructure (NCI), which is supported by the Australian Government. The theoretical calculations in this work were also supported by resources provided by the Pawsey Supercomputing Centre with funding from the Australian Government and the Government of Western Australia. For the experimental measurements, financial support from the Australian Research Council (via DP140102721, DE130100592), and the Asian Office of Aerospace Research and Development grant FA2386-15-1-4044 is gratefully acknowledged.

---

\* Electronic address: mike.ford@uts.edu.au

- <sup>1</sup> Awschalom, D. D., Bassett, L. C., Dzurak, A. S., Hu, E. L. and Petta, J. R. Quantum Spintronics: Engineering and Manipulating Atom-Like Spins in Semiconductors. *Science* 339, 1174-1179, (2013).
- <sup>2</sup> S. Castelletto, B. C. Johnson, V. Ivady, N. Stavrias, T. Umeda, A. Gali and T. Ohshima. A silicon carbide room-temperature single-photon source. *Nature Mater.* 13, 151-156, (2014).
- <sup>3</sup> Zhong, T., Kindem, J. M., Miyazono, E. and Faraon, A. Nanophotonic coherent light-matter interfaces based on rare-earth-doped crystals. *Nature Communications* 6, 8206, (2015).
- <sup>4</sup> H. Bernien, B. Hensen, W. Pfaff, G. Koolstra, M. S. Blok, L. Robledo, T. H. Taminiau, M. Markham, D. J. Twitchen, L. Childress and R. Hanson. Heralded entanglement between solid-state qubits separated by three metres. *Nature* 497, 86-90, (2013).
- <sup>5</sup> Doherty, M. W., Manson, N. B., Delaney, P. and Hollenberg, L. C. L. The negatively charged nitrogen-vacancy centre in diamond: the electronic solution. *New J. Phys.* 13, 025019, (2011).
- <sup>6</sup> Aharonovich, I., Englund, D., Toth, M. Solid-state single-photon emitters, *Nature Photonics*, 2016, 10, 631.
- <sup>7</sup> Toan Trong Tran, Kerem Bray, Michael J. Ford, Milos Toth and Igor Aharonovich, Quantum emission from hexagonal boron nitride monolayers, *Nat. Nano.* 11, 37 (2016).
- <sup>8</sup> Toan Trong Tran, Christopher Elbadawi, Daniel Totonjian, Charlene J. Lobo, Gabriele Grosso, Hyowon Moon, Dirk R. Englund, Michael J. Ford, Igor Aharonovich, and Milos Toth, Robust Multicolor Single Photon Emission from Point Defects in Hexagonal Boron Nitride, *ACS Nano* 10, 7331 (2016).
- <sup>9</sup> Nicholas R. Jungwirth, Brian Calderon, Yanxin Ji, Michael G. Spencer, Michael E. Flatte, and Gregory D. Fuchs, Temperature Dependence of Wavelength Selectable Zero-Phonon Emission from Single Defects in Hexagonal Boron Nitride, *Nano Lett.* 16, 6052 (2016).
- <sup>10</sup> Zav Shotan, Harishankar Jayakumar, Christopher R. Consideine, Mazena Mackoite, Helmut Fedder, Jorg Wrachtrup, Audrius Alkauskas, Marcus W. Doherty, Vinod M. Menon, and Carlos A. Meriles, Photoinduced Modification of Single-Photon Emitters in Hexagonal Boron Nitride, *ACS Photonics* 2016, 3, 2490.
- <sup>11</sup> Annemarie L. Exarhos, David A. Hopper, Richard R. Grote, Audrius Alkauskas, and Lee C. Bassett, Optical Signatures of Quantum Emitters in Suspended Hexagonal Boron Nitride, *ACS Nano* 2017, 11, 3328.
- <sup>12</sup> Mehran Kianinia, Sherif Abdulkader Tawfik, Blake Regan, Toan Trong Tran, Michael J. Ford, Igor Aharonovich, Milos Toth, Robust Solid State Quantum System Operating at 800 K, *ACS Photonics* 2017, 4, 768.
- <sup>13</sup> Tran, T.T., Wang, D., Xu, Z.-Q., Yang, A., Toth, M., Odom, T.W., Aharonovich, I. Deterministic Coupling of Quantum Emitters in 2D Materials to Plasmonic Nanocavity Arrays, *Nano Letters*, 2017, 17, 2634.
- <sup>14</sup> Hong, J., Jin, C., Yuan, J., Zhang, Z. Atomic Defects in Two-Dimensional Materials: From Single-Atom Spectroscopy to Functionalities in Opto-/Electronics, Nanomagnetism, and Catalysis, *Advanced Materials*, 2017, 29, 1606434.
- <sup>15</sup> Choi, S., Tran, T.T., Elbadawi, C., Lobo, C., Wang, X., Juodkazis, S., Seniutinas, G., Toth, M., Aharonovich, I. Engineering and Localization of Quantum Emitters in Large Hexagonal Boron Nitride Layers, *ACS Applied Materials and Interfaces*, 2016, 8, 29642.
- <sup>16</sup> Elbadawi, C., Tran, T.T., Kolbal, M., Sikola, T., Scott, J., Cai, Q., Li, L.H., Taniguchi, T., Watanabe, K., Toth, M., Aharonovich, I., Lobo, C. Electron beam directed etching of hexagonal boron nitride, *Nanoscale*, 2016, 8, 16182.
- <sup>17</sup> Martinez, L.J., Pelini, T., Waselowski, V., Maze, J.R., Gil,

- B., Cassaboais, G., Jacques, V. Efficient single photon emission from a high-purity hexagonal boron nitride crystal, *Phys. Rev. B.*, 2016, 94, 121405.
- <sup>18</sup> Tran, T.T., Zachreson, C., Berhane, A.M., Bray, K., Sandstrom, R.G., Li, L.H., Taniguchi, T., Watanabe, K., Aharonovich, I., Toth, M. Quantum Emission from Defects in Single-Crystalline Hexagonal Boron Nitride, *Physical Review Applied*, 2016, 5, 034005.
  - <sup>19</sup> Nathan Chejanovsky, Mohammad Rezai, Federico Paolucci, Youngwook Kim, Torsten Rendler, Wafa Rouabeh, Felipe Favaro de Oliveira, Patrick Herlinger, Andrej Denisenko, Sen Yang, Ilja Gerhardt, Amit Finkler, Jurgen H. Smet, and Jorg Wrachtrup, Structural Attributes and Photodynamics of Visible Spectrum Quantum Emitters in Hexagonal Boron Nitride, *Nano Lett.* 2016, 16, 7037.
  - <sup>20</sup> T. Q. P. Vuong, G. Cassaboais, P. Valvin, A. Ouerghi, Y. Chassagneux, C. Voisin, and B. Gil, Phonon-Photon Mapping in a Color Center in Hexagonal Boron Nitride, *Phys. Rev. Lett.* 2016, 117, 097402.
  - <sup>21</sup> P. Jaffrennou, J. Barjon, J.-S. Lauret, B. Attal-Trtout, F. Ducastelle and A. Loiseau, Origin of the excitonic recombinations in hexagonal boron nitride by spatially resolved cathodoluminescence spectroscopy, *Journal of Applied Physics* 102, 116102 (2007).
  - <sup>22</sup> Luc Mueur, Andrei Kanaev, Photoluminescence properties of pyrolytic boron nitride, *J. Mater. Sci.* 2009, 44, 2560.
  - <sup>23</sup> Luc Mueur, Demetrios Anglos, Jean-Pierre Petit, Jean Pierre Michel and Andrei V. Kanaev, Photoluminescence of hexagonal boron nitride: effect of surface oxidation under UV-laser irradiation, *Journal of luminescence* 127, 595 (2007).
  - <sup>24</sup> Xuebin Wang, Amir Pakdel, Chunyi Zhi, Kentaro Watanabe, Takashi Sekiguchi, Dmitri Golberg, and Yoshio Bando, High-yield boron nitride nanosheets from 'chemical blowing': towards practical applications in polymer composites, *Journal of Physics: Condensed Matter*, 24, 31 (2012).
  - <sup>25</sup> Dillon Wong, Jairo Velasco Jr, Long Ju, Juwon Lee, Salman Kahn, Hsin-Zon Tsai, Chad Germany, K. Suenaga, H. Kobayashi, and M. Koshino, Core-Level Spectroscopy of Point Defects in Single Layer h-BN, *Phys. Rev. Lett.* 108, 075501 (2012).
  - <sup>27</sup> Bing Huang, Hongjun Xiang, Jaejun Yu, and Su-Huai Wei, Effective Control of the Charge and Magnetic States of Transition-Metal Atoms on Single-Layer Boron Nitride, *PRL* 108, 206802 (2012).
  - <sup>28</sup> Sergio Azevedo, Jorge R Kaschny, Caio M C de Castilho and Fernando de B Mota, Theoretical investigation of native defects in a boron nitride monolayer, *Nanotechnology* 18, 495707 (2007).
  - <sup>29</sup> Bing Huang, and Hoonkyung Lee, Defect and impurity properties of hexagonal boron nitride: A first-principles calculation, *PHYSICAL REVIEW B* 86, 245406 (2012).
  - <sup>30</sup> O. Cretu, Y.-C. Lin, M. Koshino, L. H. G. Tizei, Z. Liu, and K. Suenaga, *Phys. Rev. Lett.* 114, 075502 (2015).
  - <sup>31</sup> S. P. Huber, E. Gullikson, R. W. E. van de Kruijs, F. Bijkerk, and D. Prendergast, Oxygen-stabilized triangular defects in hexagonal boron nitride, *PHYSICAL REVIEW B* 92, 245310 (2015).
  - <sup>32</sup> Rui Wang, Jiali Yang, Xiaozhi Wua and Shaofeng Wanga, Local charge states in hexagonal boron nitride with Stone-Wales defects, *Nanoscale*, 2016, 8, 8210.
  - <sup>33</sup> Audrius Alkauskas, Bob B Buckley, David D Awschalom and Chris G Van de Walle, First-principles theory of the luminescence lineshape for the triplet transition in diamond NV centres. *New J. Phys.* 16 (2014) 073026.
  - <sup>34</sup> Kun Huang and Avril Rhys, Theory of Light Absorption and Non-Radiative Transitions in F-Centres, *Proceedings of the Royal Society A*, Vol. 204, No. 1078, 1950.
  - <sup>35</sup> Optical Spectroscopy of Inorganic Solids
  - <sup>36</sup> Markham J J 1959 Interaction of normal modes with electron traps *Rev. Mod. Phys.* 31 956
  - <sup>37</sup> A.M. Stoneham, *Theory Of Defects In Solids* (Oxford: Oxford University Press), 1975.
  - <sup>38</sup> R. O. Jones and O. Gunnarsson, *Rev. Mod. Phys.* 61, 689 1989 .
  - <sup>39</sup> Jose M. Soler, Emilio Artacho, Julian D. Gale, Alberto Garcia, Javier Junquera, Pablo Ordejon and Daniel Sanchez-Portal, *Journal of Physics: Condensed Matter* 2002, 14, 2745.
  - <sup>40</sup> G. Kresse and J. Furthmuller, *Phys. Rev. B*, 1996, 54, 11169.
  - <sup>41</sup> J. P. Perdew, K. Burke and M. Ernzerhof, *Phys. Rev. Lett.*, 1996, 77, 3865.
  - <sup>42</sup> Troullier, N.; Martins, J. *Solid State Communications* 1990, 74, 613.
  - <sup>43</sup> P. E. Blochl, *Phys. Rev. B*, 1994, 50, 17953.
  - <sup>44</sup> Atsushi Togo and Isao Tanaka, First principles phonon calculations in materials science, *Scr. Mater.*, 108, 1-5 (2015).
  - <sup>45</sup> Jeppe Gavnholt, Thomas Olsen, Mads Engelund, and Jakob Schiøtz,  $\Delta$  self-consistent field method to obtain potential energy surfaces of excited molecules on surfaces, *Phys. Rev. B* 78, 075441.
  - <sup>46</sup> A. Hellman, B. Razaznejad, and B. I. Lundqvist, *J. Chem. Phys.* 120, 4593 2004 .
  - <sup>47</sup> J. R. Weber, W. F. Koehl, J. B. Varley, A. Janotti, B. B. Buckley, C. G. Van de Walle, and D. D. Awschalom, Quantum computing with defects, *PNAS* 107, 19 (2010).
  - <sup>48</sup> Kubo R and Toyozawa Y 1955 Application of the method of generating function to radiative and non-radiative transitions of a trapped electron in a crystal *Prog. Theor. Phys.* 13 160
  - <sup>49</sup> Alkauskas A, Lyons J L, Steiauf D and Van de Walle C G 2012 First-principles calculations of luminescence spectrum line shapes for defects in semiconductors: the example of GaN and ZnO *Phys. Rev. Lett.* 109 267401.
  - <sup>50</sup> G. Davies, Vibronic spectra in diamond *J. Phys. C: Solid State. Phys.*, 1974, 7, 3797.